BENI-SUEF UNIVERSITY JOURNAL OF BASIC AND APPLIED SCIENCES 2 (2013) 61–71

Available online at www.sciencedirect.com

SciVerse ScienceDirect

journal homepage: www.elsevier.com/locate/bjbas

Full Length Article

Adsorption of Pb(II) ions from aqueous solutions using copper oxide nanostructures

A.A. Farghali [a,*], M. Bahgat [b], A. Enaiet Allah [a], M.H. Khedr [a]

[a] Materials Science Lab, Chemistry Department, Faculty of Science, Beni-Suef University, Beni-Suef, Egypt
[b] Central Metallurgical Researches and Development Institute (CMRDI), Helwan, Egypt

ARTICLE INFO

Article history:
Received 15 November 2012
Accepted 2 January 2013
Available online 1 October 2013

Keywords:
Copper oxide
Microwave
Nanostructures
Morphology
Adsorption
Lead ions

ABSTRACT

Various morphologies of CuO nanostructures (oval, cluster, leaves, small rod, porus nanosheets) have been synthesized by novel simple method using microwave radiation. The produced CuO nanostructures were characterized by X-ray diffraction analysis technique (XRD), transmission electron microscopy (TEM), surface area analyzer (BET) and energy dispersive spectroscopy (EDS). The ability of CuO nanostructures as adsorbent was investigated for adsorptive removal of Pb(II) ions from aqueous solutions. Various physico–chemical parameters such as pH, initial metal ion concentration, and equilibrium contact time were studied. The optimum solution pH for adsorption of Pb(II) from aqueous solutions was found to be 6.5 and the optimum contact time was found to be 4 h. The adsorption isotherms were obtained using concentrations of the metal ions ranging from 100 to 300 mg/l. The adsorption process follows pseudo-second-order reaction kinetics, as well as Langmuir and Freundlich adsorption isotherms. The maximum capacity of oval, cluster, leaves, small rod and porus nanosheets CuO nanostructures for Pb^{2+} are 125, 116, 117, 120 and 115 mg/g. This study revealed that CuO nano structures was an effective adsorbent for removal of Pb(II) ions from aqueous solutions.

1. Introduction

Water pollution by heavy metal ions has become a serious environmental issue especially due to their toxicity and tendency to bioaccumulation (Sari and Tuzen, 2008; Heidari et al., 2009). The heavy metal ions are not only toxic to living organisms in water, but also cause harmful effects to land animals including humans through food chain transfers. In living organisms, heavy metal ions can particularly bind to nucleic acids, proteins, and small metabolites. The contaminated organic cells are altered or missed their biological functions with losing the homeostatic control of essential metals, resulting in fatal health problems (Liu et al., 2008). The release of large quantities of heavy metals into the natural

* Corresponding author.
E-mail address: d_farghali@yahoo.com (A.A. Farghali).
Peer review under the responsibility of Beni-Suef University

Production and hosting by Elsevier

2314-8535/$ – see front matter Copyright 2013, Beni-Suef University. Production and hosting by Elsevier B.V. All rights reserved.
http://dx.doi.org/10.1016/j.bjbas.2013.01.001

environment e.g. irrigation of agricultural fields by using sewage has resulted in a number of environmental problems and due to their non-biodegradability and persistence, can accumulate in the food chain, and thus may pose a significant danger to human health (Alvarez-Ayuso, Garcia-Sanchez et al., 2003; Ruparelia et al., 2008). Pb(II) is a highly toxic substance, exposure to which can produce a wide range of adverse health effects for both adults and children. Very low levels of exposure to young children under the age of six can result in reduced IQ, learning disabilities, attention deficit disorders, behavioral problems, stunted growth, impaired hearing, and kidney damage. At high levels of exposure, a child may become mentally retarded, fall into a coma, and even die from lead poisoning. In adults, lead can increase blood pressure and cause fertility problems, nerve disorders, muscle and joint pain, irritability, and memory or concentration problems (NSC, 2007). Therefore, it is necessary to eliminate such hazardous heavy metal ion in wastewater before discharging it into the ecosystem. The tolerance limits for heavy metal concentration in potable water and discharge into inland surface waters is shown in Table 1 (Naiya et al., 2009).

The contamination of wastewaters and surface waters by toxic heavy metals is worldwide environmental problem. These toxic metal ions commonly exist in process waste streams from mining operations, metal plating facilities, power generation facilities, electronic device manufacturing units, and tanneries. Because of economic and environmental factors, the removal and recovery of heavy-metal ions from industrial wastewater have been a significant concern in most industrial branches (Ngomsik et al., 2009; Yin et al., 2010). The most commonly applied physicochemical treatment methods are: (i) precipitation as hydroxides, carbonates or sulfides and subsequent liquid-solids separation by gravity settling, and flotation or filtration, (ii) sorption (adsorption, ion exchange), (iii) membrane processes, (iv) electrolytic recovery and (v) liquid–liquid extraction (Afkhami and Conway, 2002; Afkhami et al., 2008; Hota et al., 2008; Wang and Chen, 2009). However, each method has its merits and limitations in application and they are often limited by technical and economical issues (Pacheco et al., 2006; Wang and Chen, 2009). Also these methods have significant disadvantages, which are for instance incomplete removal, high-energy requirements, production of toxic sludge or waste products that also require disposal and become economically unviable for the removal of heavy metals at lower concentrations (Aklil et al., 2004). The adsorption process is arguably one of the more popular methods for the removal of heavy-metal ions because of its simplicity, convenience, and high removal efficiency (Luisa Cervera et al., 2003; Santos Yabe and de Oliveira, 2003; Afkhami et al., 2007). The adsorption process with activated carbon is attractive to many scientists because of the effectiveness of the removal of heavy-metal ions at trace quantities (Wang and Kuo, 2008; Rao et al., 2009). However, the process has not been used extensively because of its high cost (Dias et al., 2007; Wang and Kuo, 2008; Rao et al., 2009) Therefore, the use of low-cost materials as sorbents for metal removal from wastewater has been a focus. Using low-cost biosorbents such as agricultural wastes, clay materials, biomass, and seafood processing wastes may be an alternative wastewater technology because they are inexpensive and capable of removing trace levels of heavy-metal ions (Jiang et al., 2009; Munagapati et al., 2010). However, to improve their absorption capacity and enhance the separation rate, the design and exploration of novel adsorbents are still necessary.

Recently, application of nanoparticles for the removal of pollutants has come up as an interesting area of research. The unique properties of nanosorbents are providing unprecedented opportunities for the removal of metals in highly efficient and cost-effective approaches, and various nanoparticles and dendrimers have been exploited for this purpose (Jiang et al., 2009; Afkhami and Moosavi, 2010; Yang et al., 2011). Nanoparticles exhibit good adsorption efficiency especially due to higher surface area and greater active sites for interaction with metallic species. Furthermore, adsorbents with specific functional groups have been developed to improve the adsorption capacity (Turker, 2007).

Nanoscale metal oxides potentially offer a more cost efficient water treatment and remediation technology due to their size and adsorption efficiency (Zhang, 2003; Engates and Shipley, 2010).

CuO was found to be an effective adsorbent for heavy metals as arsenic because it did not require pH adjustments or oxidation of As(III) to As (V) and it performed well in the presence of competing anions. These studies attributed the effective removal of arsenic by CuO to its high point of zero charge. CuO's point of zero charge is estimated to be 9.4 ± 0.4 (Martinson and Reddy, 2009).

The present work aims to prepare CuO nanoparticles with different morphologies with simple and facile method and test the effect of the morphology of the prepared nanoparticles on their adsorption efficiency.

2. Materials and methods

Different morphologies of nano-sized particles of copper (II) oxide were prepared using microwave heating technique, (Black and Decker, MZ3000PG/MZ3000PGSA/England). The prepared nanostructures were:

Table 1 – Tolerance limits for Pb(II) metal ions concentration in drinking water and discharge into inland surface waters.

Heavy metal	IS 10500 1992			EPA	WHO
	Drinking water (mg/l)	Discharge in inland surface water (mg/l)	Discharge in public sewers (mg/l)	Drinking water (mg/l)	Drinking water (mg/l)
Pb(II)	0.05	0.10	0.10	0.015	0.01

- Sample A: oval shaped CuO
- Sample B: cluster shaped CuO
- Sample C: leaves shaped CuO
- Sample D: small nanorods CuO
- Sample E: porous nanosheets

2.1. Preparation of the CuO oval shape and cluster shape

For simple synthesis of CuO oval shaped nanoparticles, 200 ml of 0.1 M solution of copper nitrate [$Cu(NO_3)_2 \cdot 3H_2O$] was mixed with 0.1 M NaOH solution and the solution was heated using microwave radiation of power 900 Watt for 5 min. After the reaction was completed, the precipitate was filtered, washed with distilled water and finally dried at 80 °C for 5 h. The cluster shape was obtained by repeating the same procedure and applying the precipitation step at 100 °C for copper nitrate solution.

2.2. Preparation of the CuO nanoleaves and small nanorods

The CuO nanoleaves were prepared using Diethylene glycol (DEG) assisted microwave process. Specific amount of $CuSO_4 \cdot 5H_2O$ was dissolved in de-ionized water under stirring, after 5 min, 20 ml DEG and 20 ml of 2 M NaOH solution were introduced into the above aqueous solution under continuous stirring. The solution was heated using microwave radiation with power 450 W for 10 min. After the reaction was completed, the precipitate was filtered, washed with distilled water and finally dried at 80 °C for 5 h. The small nanorods shape was obtained by repeating the same procedure and applying the precipitation step at 100 °C for copper sulphate solution.

2.3. Preparation of the CuO porous nano sheets

3.6 g of $Cu(NO_3)_2 \cdot 3H_2O$ was dissolved in 300 ml deionized water and then 30 ml of DEG was poured into the solution. After DEG uniformly dispersed in the solution, NaOH pellets were added. The solution was stirred for 2 h then; the blue suspension was heated using microwave radiation with power 900 W for 5 min. After the reaction was completed, all precipitate was filtered, washed with distilled water and finally dried at 80 °C for 5 h.

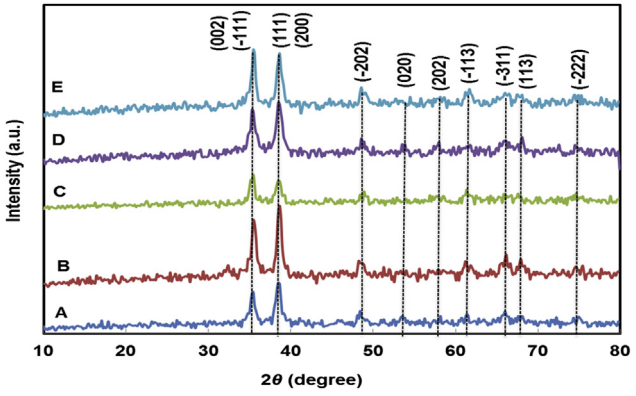

Fig. 1 – XRD patterns of synthesized nano-sized CuO powder with different morphologies (A) oval shape, (B) leaves shape, (C) cluster shape, (D) small nano rods, (E) porous nanosheet.

2.4. Characterization of the prepared nano-materials

Morphology and microstructure of CuO nanostructures were studied using transmission electron microscope (JEOL JEM-2100 TEM). X-ray diffraction technique using X-ray phase analysis (PW 1730) with nickel filtered Cu radiation at 40 kV and 30 mA, and EDX (JEOL JED-2300 SEM) were used to investigate the crystalline phase and chemical composition of the prepared samples. The average crystal size was calculated using the XRD peaks with the application of a software computer programme TOPAZ2 depending on the following Scherer's formula (Cullity, 1978).

$$D = 0.9\lambda/\beta \cos\theta \quad (1)$$

where D is the crystallite size, λ is the X-ray wave length, β is the broadening of the diffraction peak and θ is the diffraction angle.

The BET surface area for the prepared samples was determined using a Quantachrome NOVA Automated Gas Sorption System Report.

2.5. Batch removal experiments for adsorption of lead Pb(II) ions

The adsorption of lead was studied by a batch operation at room temperature. The batch mode adsorption was selected due to its simplicity.

2.6. Effect of PH on adsorption of Pb(II) ions

The adsorption experiments were carried out in a series of 250 ml Erlenmeyer flasks containing 0.1 g nano structured CuO and 50 ml of 50 mg/l Pb ions solution at serial pH values (3–6.5). The prepared samples were shaken with mechanical shaker for 6 h. Then solid/liquid phases were separated by filtration. The concentration of the Pb(II) ions before and after adsorption was determined using Atomic Absorption mass spectrometry (Thermo electron Ltd., solar House Cambridge. UK, Solar M_6A.A.spectrometer). The adsorbed amount of metal ions onto the CuO nanostructures was calculated according to the following equations:

$$Q = (C_0 - C_t)/C_0 \times 100 \quad (2)$$

where Q is the adsorptivity (%), C_0 and C_t are the concentration of metal ions before and after adsorption in mg, V is the volume of metal ions solution in liter scale, and W is the weight of the adsorbent in gram scale.

2.7. Effect of contact time on adsorption of Pb ions (II)

Typically, 0.1 g nano structured CuO was added into each flask containing 50 ml of Pb(II) ion solution of 50 mg/l at a pH value of 6.5. The prepared samples were shaken with mechanical shaker for different intervals of time (from 1 to 6 h). After a desired time, the CuO was removed from the solution by

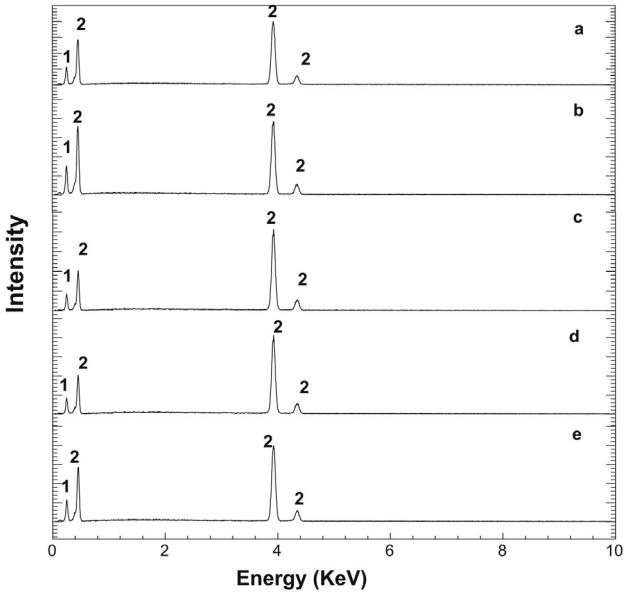

Fig. 2 – EDX patterns of synthesized nano-sized CuO powder with different morphologies where 1:2 (O:Cu) (a) oval shape, (b) leaves shape, (c) cluster shape, (d) small nano rods, (e) porous nanosheet.

filtration. The residual Pb(II) ion concentration was determined by Atomic Absorption spectrophotometer.

2.8. *Effect of initial metal ion concentration on adsorption of Pb(II) ions and adsorption isotherm*

Typically, 0.1 g nano structured CuO was added into each flask containing 50 ml of Pb(II) ion solutions with various initial metal ion concentrations (from 100 mg/l to 300 mg/l) at pH 6.5. All the flasks were shaken with mechanical shaker. At the end of the equilibrium period, the CuO was removed from the solution by filtration. The residual Pb(II) ion concentration was determined by Atomic Absorption spectrophotometer. The amount of Pb(II) ions adsorption at equilibrium q_e (mg/g) was calculated from the following equation:

$$q_e = V(C_0 - C_e)/W \quad (3)$$

where q_e is the equilibrium adsorption capacity of adsorbent in mg (metal)/g (adsorbent), C_0 is the concentration of metal ions before adsorption in mg/l, C_e is the equilibrium concentration of metal ions in mg/l, V is the volume of metal ions solution in liter scale, and W is the weight of the adsorbent in gram scale.

2.9. *Adsorption kinetics experiment*

Kinetic experimental procedures were identical to the equilibrium tests. The effect of contact time on the amounts of adsorbed Pb(II) ions on the adsorbent materials at any time, t, were calculated from the concentrations in solutions before and after adsorption. At any time, the amount of adsorbed Pb(II) ions (mg/g) onto the adsorbent materials was calculated from the mass balance equation as follows:

$$Q_t = V(C_0 - C_t)/W \quad (4)$$

where Q_t is the amount of adsorbed Pb(II) ions on the adsorbent materials at any time (mg/g); C_0 is the concentration of metal ions before adsorption in mg/l, C_t is the concentration of metal ions after adsorption in mg/l, V is the volume of metal ions solution in liter scale, and W is the weight of the adsorbent in gram scale.

3. Results and discussion

3.1. *Characterization*

XRD patterns (Fig. 1) confirm that Nano-sized copper oxide powder was successfully prepared by precipitation method using microwave heating technique. It is clearly seen that XRD patterns for all samples are identical to the single phase of CuO with a monoclinic structure with two main peaks at 2θ value 35.5 and 38.6. No other peaks are observed, indicating the high purity and well crystallinity of the obtained samples.

The average crystallite size was calculated using X-ray peak broadening technique of the main peak and was found to be 19.4, 12.9, 13.1, 9.4, 11.5 nm for sample A, B, C, D and E, respectively.

The chemical composition of the nanostructures was analyzed using energy dispersive spectroscopy (EDS) where its spectrum reveals that the atomic ratio of Cu:O is equal to 1:1 in the five samples (Fig. 2).

TEM images of the produced CuO nanostructures are presented in Fig. 3(a–f), where the different morphologies that be achieved simply by changing the preparation condition can be clearly observed. Fig. 3 (a) depicts the typical TEM image of the oval shaped CuO nanoparticles where small spherical nanoparticles with 20 nm in size are aggregated to form oval shaped CuO with a width range from 150 to 200 nm and a length range from 350 to 400 nm with tapered sides. Fig. 3 (b) shows TEM. image of a cluster shaped CuO nanoparticles which has a crystal size about 13 nm and consists of spherical nanoparticles with diameter about 5–8 nm, this cluster length ranges from 110 to 250 nm. Fig. 3(c) shows TEM image of leaves structure morphology with a width range from 100 to 200 nm and with a length range from 250 to 450 nm and serrated edges. Fig. 3(d) illustrates the TEM image of nano rod shape with a diameter range from 6 to 12 nm and a length range from 50 to 70 nm. Fig. 3(e) shows TEM image of porous nanosheets structures with a length range from 145 to 230 nm and a width range from 70 to 100 nm with a thickness of 1 nm and pores diameter ranging from 0.8 to 2 nm as it appear in Fig. 3(f).

The BET method is applied to evaluate the specific surface area of the CuO nanostructures. The obtained specific surface area for oval, cluster, leaves, small nanorods and porous nanosheets are 5.62, 2.95, 14.35, 3.598 and 4.774 m^2/g, respectively.

3.2. *Effect of the process temperature*

For sample A, C, B and D, the adding of NaOH temperature has a clear influence on the shape and size of CuO nanocrystal. As it can be seen from Fig. 3(a), the oval shape has crystal size of 19.4 nm with dense agglomerated nanoparticles when NaOH added at mild reaction condition. Adding NaOH to boiling

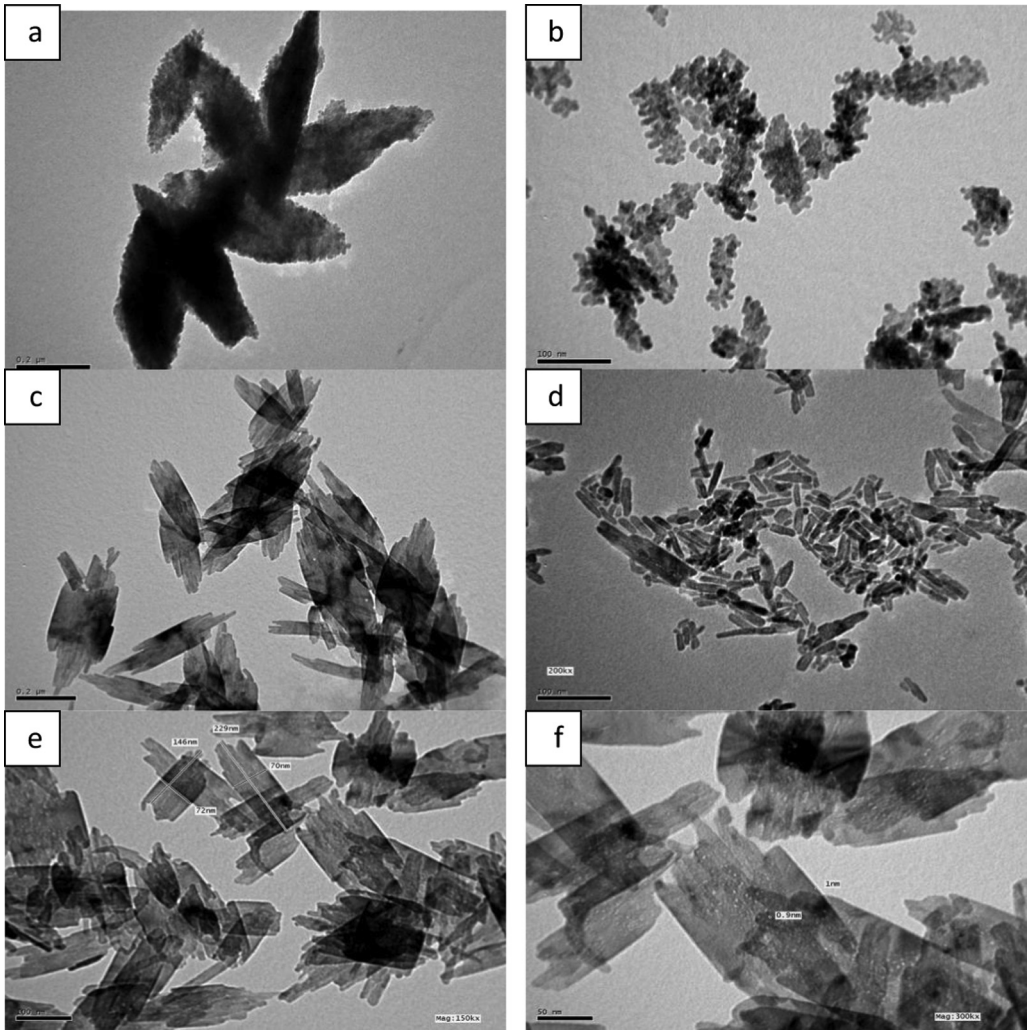

Fig. 3 – TEM images of nano-sized copper oxide powder (a) oval shape, (b) cluster shape, (c) leaves shape, (d) rod shape, (e–f) porous nano sheet.

solution with 100 °C yields cluster shape of identified spherical nanoparticles with crystal size of 12.9 nm as shown in Fig. 3(b).

Also as shown from Fig. 3(c), the agglomerated leaves shape with crystal size of 13.1 nm, which is formed when NaOH was added at mild reaction condition, changed into homogenous nanorod with crystal size of 9.4 nm when NaOH was added to boiling solution with 100 °C as shown in Fig. 3(d) The difference in crystal sizes is due to temperature degree of CuO particles were low at mild reaction solution while higher temperature caused higher reaction rate which might cause large amount of nuclei formation in a short time without aggregation. On the other hand, nucleation and growth rate of condition which led to aggregation of CuO particles to form larger size of the crystals (Zhu et al., 2004). While higher temperature increased the reaction rate leading to large amount of nuclei formation in a short time without aggregation.

3.3. *Effect of DEG*

The high polarizability of DEG makes this solvent an excellent microwave absorbing agent leading to a high heating rate and a significantly shorter reaction time (Niederberger and Pinna, 2009).

Furthermore, DEG stabilizes the particle surfaces during nucleation and crystallization, and therefore prevents particle growth and aggregation. This stabilizing effect of multidentate and high-boiling alcohols (so-called polyols, e.g. diethylene glycol/DEG, ethylene glycol, glycerine) has already been described and used to prepare a wide range of nanoscale materials, including elemental metals, oxides, sulfides or fluorides (Feldmann et al., 2006). It is shown that samples C, D and E have smaller crystal size than that of A and B which are prepared without adding DEG.

3.4. *Adsorption studies of Pb(II) ion on CuO nanostructures*

3.4.1. *Effect of initial pH*

pH is an important factor affecting the removal of cations from aqueous solutions. The dependence of metal sorption on pH is related to both the metal chemistry in the solution and the ionization state of the functional groups of the sorbent

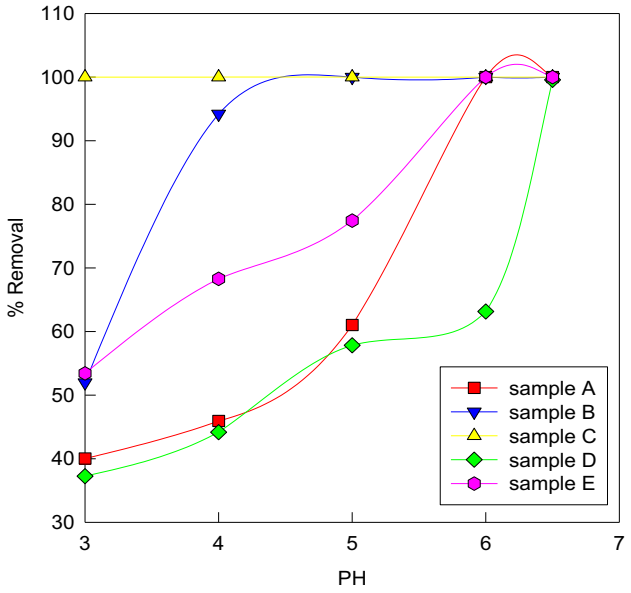

Fig. 4 – Percentage of metal ions removal at different pHs. Conditions: 0.1 g adsorbent, 50 ml of 50 mg/l of Pb^{+2} ions, agitation time of 6 h.

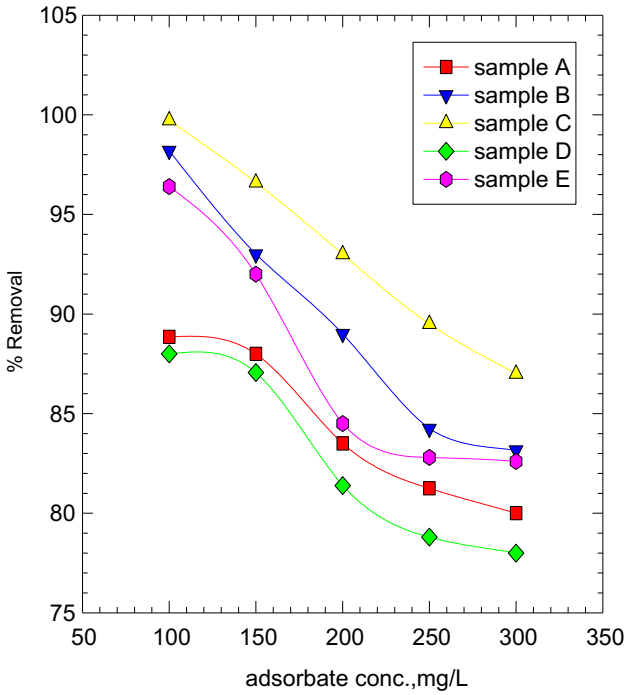

Fig. 6 – Percentage of metal ions removal at different adsorbate concentration. Conditions: 0.1 g adsorbent, 50 ml of Pb^{+2} ions, pH, 6.5 agitation time of 24 h.

which affects the availability of binding sites (Heidari et al., 2009; Ngomsik et al., 2009).

In order to evaluate the influence of this parameter on the adsorption of Pb(II) ions, the experiments were carried out with the pH range of (3, 4, 5, 6, 6.5). The pH range was chosen as (3–6.5) in order to avoid precipitation of Pb in the form of metal hydroxides. The effect of pH on adsorption efficiencies is shown in Fig. 4 Removal of Pb(II) ions increases gradually with increasing solution pH from 3 to 6.5 and the maximum value was reached at pH of 6.5, So it was considered as optimum condition. Similar behavior has been reported by many authors (Zhang et al., 2001; Mohapatra and Anand, 2007) for the uptake of metal ions on various adsorbents. At low pH, the percentage adsorption is low for these metal ions, as large quantities of protons compete with metal cations for the adsorption sites. According to Low et al. (1995), at low pH value, the surface of the adsorbent, would be closely associated with hydronium ions (H_3O^+) and hold mainly protonated sites as a result, the surface maintains a net positive charge. Hence it hinders the access of the metal ions to the surface functional group. Consequently the percentage of metal ion removal may decrease at low pH. The positive charge on adsorbent surface, however, gradually decreases as pH increases, thus reducing the electrical repulsion between sorbing surface and cations. Moreover, lower H^+ concentration also favors cation sorption by mass action. For example, the adsorption of bivalent cations such as M^{2+} on iron oxide can be written as:

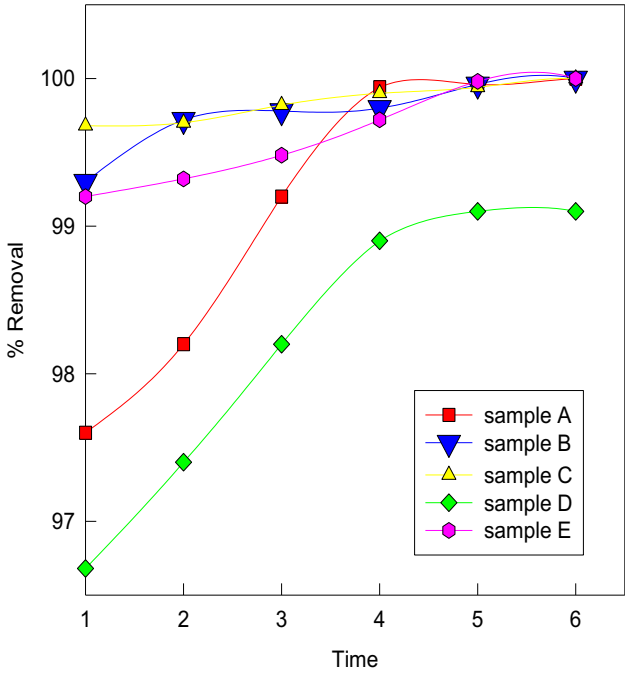

Fig. 5 – Percentage of metal ions removal at different times. Conditions: 0.1 g adsorbent, 50 ml of 50 mg/l of Pb^{+2} ions, pH,6.5.

$$FeOH_2^+ + M^{2+} \rightarrow FeOM^+ + 2H^+$$

Lowering H^+ concentration will drive this reaction toward the right-hand side and favor the sorption of M^{2+} by increasing pH (Mohapatra et al., 2010).

3.4.2. *Effect of contact time*

The importance of contact time comes from the need for identification of the possible rapidness of binding and removal processes of the tested metal ions by the synthesized

adsorbents and obtaining the optimum time for complete removal of the target metal ion.

The analysis of batch adsorption of metal ions was carried out in 30 min steps and the concentration of each sample was measured by atomic absorption spectroscopy after 6 h contact time. The data for adsorption experiment were replicated three times and the results were averaged. The results were recorded and the time profile of heavy-metal ions adsorption was plotted as shown in Fig. 5. There is an increase in adsorption with increase in contact time and maximum adsorption takes place at 4 h and again after 4 h contact time there was no further adsorption. This may be due to the fact that initially all adsorbent sites were vacant and the solute concentration gradient was high. Later, the lead uptake rate by adsorbent was decreased significantly, due to the decrease in number of adsorption sites as well as lead concentration. Therefore, the optimum contact time for adsorption of the heavy metals was considered to be 4 h.

3.4.3. *Effect of initial Pb(II) ions concentration with different morphologies of CuO*

The Pb(II) ion removal performance of the CuO was evaluated as a function of the initial Pb(II) ion concentration (from 100 mg/l to 300 mg/l) at a pH value of 6.5. In this study, the adsorption time was fixed at 24 h to achieve an equilibrium state. As illustrated in Fig. 6, the Pb(II) ion adsorptivity (% removal) depended on the initial Pb(II) ions concentration. Where the adsorptivity decreases with the increasing of initial lead concentration. This is a result of the increase in the driving force from the concentration gradient. The results given in Fig. 6 show that the adsorptivity toward CuO nanostructures were in the order leaves > cluster > porous nanosheets > oval > small nanorods within the studied range of initial metal ion concentrations.

Leaves structure has obviously better removal ability than the other samples due to very large surface area. Although cluster structure and porous nanosheet structure have smaller surface area than oval structure, they have higher activity toward adsorption of lead. This may be due to unique structure of cluster shape which is consisted of aggregated spheres and porosity of porous nanosheets.

3.5. *Adsorption isotherm and kinetics of adsorption of Pb(II) metal ions onto CuO nanostructures*

3.5.1. *Adsorption isotherm*

The relationship between the amount of a substance adsorbed per unit mass of adsorbent at constant temperature and its concentration in the equilibrium solution is called the adsorption isotherm. Adsorption isotherm is important to describe

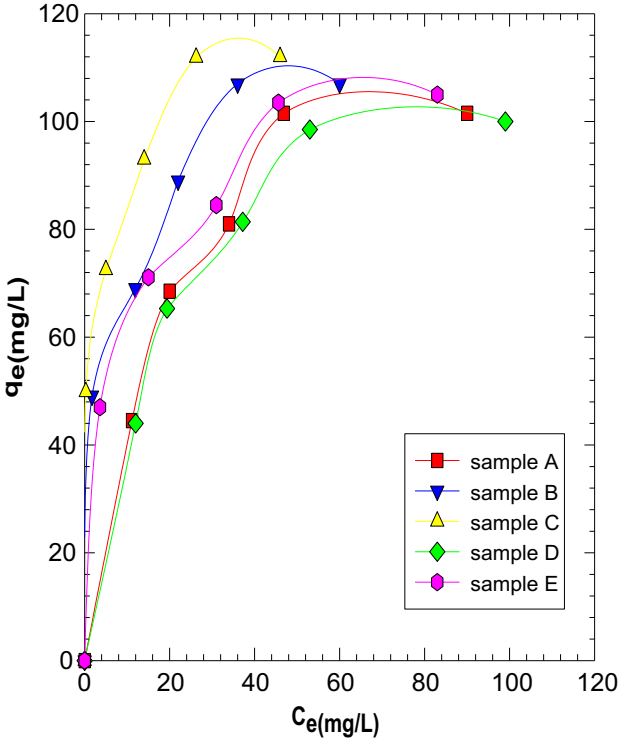

Fig. 7 – Adsorption isotherms of Pb(II) metal ions onto CuO nanostructures.

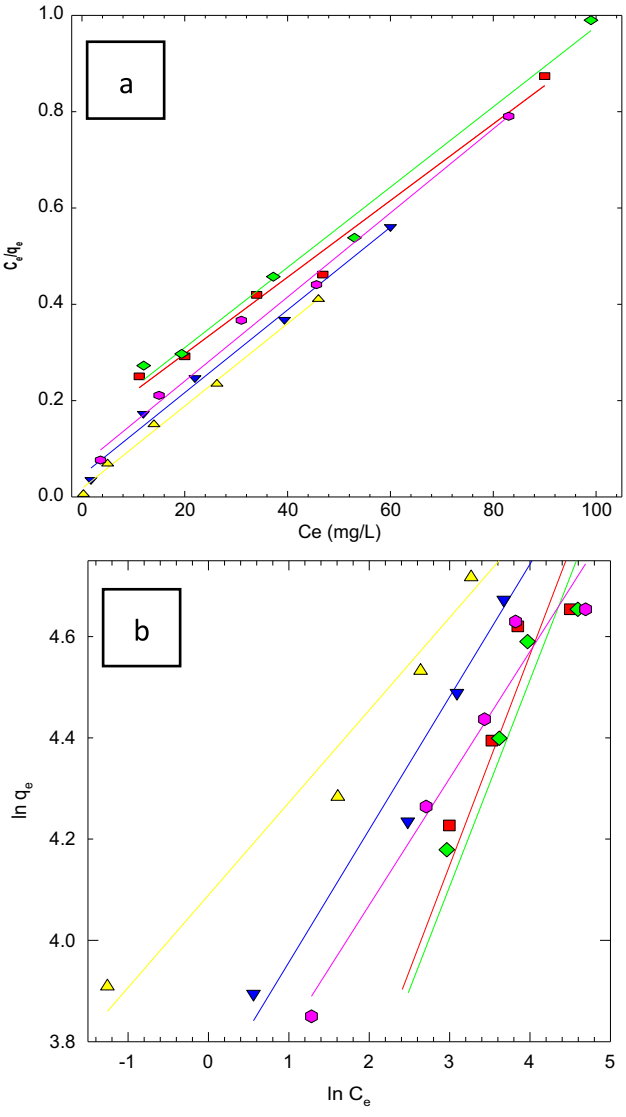

Fig. 8 – Langmuir (a) and Freundlich (b) isotherms for Pb(II) metal ions onto CuO nanostructures.

Table 2 – Isotherm parameters for removal of Pb(II) metal ions onto CuO nanostructures.

Isotherms	Parameters	Copper oxide nanostructures				
		Sample A	Sample B	SampleC	Sample D	Sample E
Langmuir	q_0 (mg/g)	125	116	117	120	115
	K_L (l/mg)	0.561	0.191	0.496	0.0581	0.132
	R_L	0.056	0.0171	0.0066	0.054	0.024
	R^2	0.996	0.989	0.994	0.989	0.992
Freundlich	K_F (mg/g (l/mg)1/n)	18.155	40.2	59.68	17.84	35.44
	n	2.402	3.815	5.49	2.45	4
	R^2	0.903	0.965	0.967	0.919	0.952

how solutes interact with the sorbent. Developing an appropriate isotherm model for adsorption is essential to the design and optimization of adsorption processes. Several isotherm models have been developed for evaluating the equilibrium adsorption of compounds from solutions, such as Langmuir, Freundlich, Redlich–Peterson, Dubinin–Radushkevich, Sips, and Temkin (Dabrowski, 2001).

Since the more common models used to investigate the adsorption isotherm are Langmuir and Freundlich equations, the experimental results of this study are fitted with these two models. The equilibrium adsorption isotherms are important in determining the adsorption capacity of Pb(II) metal ions and diagnose the nature of adsorption onto the CuO nanostructures.

The equilibrium adsorption capacity of adsorbent was calculated by the following equation:

$$q_e = V(C_0 - C_e)/W \quad (5)$$

where q_e is the equilibrium adsorption capacity of adsorbent in mg metal/g adsorbent, C_0 is the initial concentration of the metal ions in mg/l, C_e is the equilibrium concentration of metal ions in mg/l, V is the volume of metal ions solution in L, and W is the weight of the adsorbent in g. The equilibrium adsorption of metal ion solutions by adsorbent was measured (50 ml of 100–300 mg/l) after equilibrium time.

The adsorption isotherms of Pb(II) metal ions on the CuO nanostructures are shown in Fig. 7. As shown in Fig. 7, equilibrium uptake increased with Pb(II) metal ions concentration. This is a result of the increase in the driving force from the concentration gradient. In the same conditions if the concentration of Pb(II) metal ions is higher, the active sites of the CuO nanostructures are surrounded by many more Pb(II) metal ions, and the process of adsorption would carry.

The most widely used Langmuir equation, which is valid for monolayer sorption on a surface with a finite number of identical sites, is given by (Langmuir, 1918).

$$C_e/q_e = 1/q_0K_L + (1/q_0)C_e \quad (6)$$

where C_e (mg/l) is the equilibrium concentration, q_e (mg/g) is the amount of adsorbate adsorbed per unit mass of adsorbate, and q_0 and K_L are the Langmuir constants related to the adsorption capacity and the rate of adsorption, respectively. When C_e/q_e was plotted against C_e, a straight line with a slope of $1/q_0$ was obtained (Fig. 8(a)), indicating that the adsorption of Pb(II) metal ions on the CuO nanostructures follows the Langmuir isotherm. The Langmuir constants K_L and q_0 were calculated from this isotherm and their values are listed in Table 2. Another important parameter, R_L, called the separation factor or the equilibrium parameter, is evaluated in this study and determined from the following relation (Hall et al., 1966)

$$R_L = 1/[1 + K_LC_0] \quad (7)$$

Here, K_L is the Langmuir constant (l/mg) and C_0 (mg/l) is the highest Pb(II) metal ions concentration. The value of R_L indicates whether adsorption will be unfavorable adsorption onto the CuO were ($R_L > 1$), linear ($R_L = 1$), favorable ($0 < R_L < 1$) or irreversible ($R_L = 0$). R_L values for Pb(II) metal ions were calculated and its value was less than 1 and greater than zero indicating favorable adsorption (Table 2).

The Freundlich isotherm model is an empirical relationship describing the adsorption of solutes from a liquid to a solid surface, and assumes that different sites with several adsorption energies are involved. The linear form of the Freundlich equation is:

$$\ln q_e = \ln K_F + (1/n)\ln C_e \quad (8)$$

where q_e is the amount adsorbed at equilibrium (mg/g) and C_e is the equilibrium concentration of Pb(II) metal ions. K_F and n are Freundlich constants, where K_F (mg/g (l/mg)$^{1/n}$) is the adsorption capacity of the adsorbent and n giving an indication of how favorable the adsorption process. The slope $1/n$ ranging between 0 and 1 is a measure of adsorption intensity or surface heterogeneity, becoming more heterogeneous as its value gets closer to 0 (Haghseresht and Lu, 1998).

The plot of ln q_e versus ln C_e (Fig. 8 (b)) gives straight lines with slope $1/n$. Fig. 8 (b) shows that the adsorption of Pb(II) metal ions also follows the Freundlich isotherm. Accordingly, Freundlich constants (K_F and n) were calculated and listed in Table 2.

3.5.2. *Kinetics analyses*

The dynamics of the adsorption process in terms of the order and the rate constant can be evaluated using the kinetic adsorption data. The process of Pb(II) ions removal from an aqueous phase by adsorbent can be explained by using kinetic models and examining the rate-controlling mechanism of the adsorption process such as chemical reaction, diffusion control and mass transfer. The kinetic parameters are useful in predicting the adsorption rate which can be used as important information in designing and modeling of the adsorption operation. The kinetics of removal of metal ions are explicitly explained in the literature using pseudo-first-order, pseudo-second-order and intraparticle diffusion kinetic models.

In order to investigate the mechanisms of metal adsorption process, the linearized equations of pseudo-first-order, pseudo-second-order and intraparticle diffusion kinetic models were applied and the results were shown in Fig. 9. The pseudo-first-order kinetic model assumes that the binding is originated from physical adsorption and the equation is given as:

$$\ln(q_e - q) = \ln(q_e) - k_1 t \quad (9)$$

where q_e and q are the amounts of Pb(II) ions adsorbed on the CuO nanostructures in mg(metal)/g(adsorbent) at equilibrium and at time t respectively, and k_1 is the rate constant of the pseudo first-order model for the adsorption (min^{-1}) (Demirbas et al., 2009). The values of q_e and k_1 can be determined from the intercept and the slope of the linear plot of ln ($q_e - q$) versus t.

The pseudo second-order model is based on chemical adsorption (chemisorption) and the equation is given as:

$$(t/q) = 1/(k_2 q_e^2) + (t/q_e) \quad (10)$$

where q_e and q follow the same definition as the pseudo first-order model and k_2 is the rate constant of the pseudo second-order model for adsorption (g/mg min) (Demirbas et al., 2009). The slope and intercept of the linear plot of t/q against t yielded the values of q_e and k_2. Additionally, the initial adsorption rate h (mg/g min) can be determined from $h = k_2 q_e^2$. Since neither the pseudo first-order nor the second-order model can identify the diffusion mechanism, the kinetic results were analyzed by the intraparticle diffusion model to elucidate the diffusion mechanism, which model is expressed as:

$$q = k_i t^{1/2} + C \quad (11)$$

where C is the intercept and k_i is the intraparticle diffusion rate constant (mg/g $min^{1/2}$), which can be evaluated from the slope of the linear plot of q versus $t^{1/2}$ (Weber and Morris, 1963).

The results of Fig. 9 are fitted using pseudo-first- and second-order models and intraparticle diffusion model. The fit of these models was checked by each linear plot of ln ($q_e - q_t$) versus t, (t/q_t) versus t and q_t versus $t^{1/2}$, respectively as shown in Fig. 9 (a–c). Table 3 presented the coefficients of the pseudo-first and second-order adsorption kinetic models and the intraparticle diffusion model.

By comparing to the regression coefficients for each expression. First order rate expression and intraparticle diffusion model is not fully valid for the present systems due to low correlation coefficients. Hence for the first order rate expression, the experimental q_e values do not agree with the calculated ones obtained from the linear plots. A good agreement of the experimental data with the second order kinetic model was observed for different adsorbent which is presented in Fig. 9(b). Correlation coefficients for the linear plots using the pseudo-second order model are superior (in most cases >0.99), and theoretical and experimental q_e values show excellent agreement.

Therefore, it is likely that the sorption of Pb(II) ions by CuO nanostructures is kinetically controlled as a second order reaction rather than a first order process. The pseudo-second order model assumes chemical sorptions as the rate-limiting process.

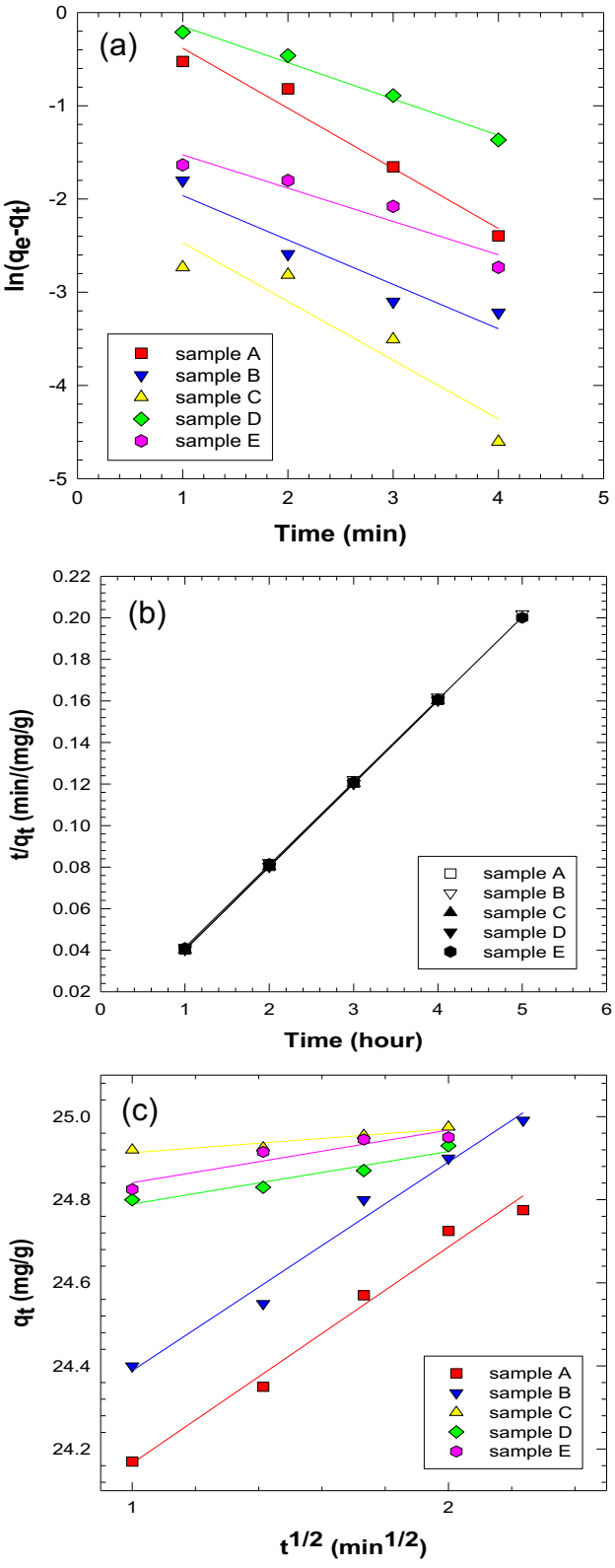

Fig. 9 – Regressions of kinetic plots for CuO nanostructures: (a) pseudo-first-order model, (b) pseudo-second-order model and (c) intraparticle diffusion model.

Table 3 – Coefficients of pseudo-first and second-order adsorption kinetic models and intraparticle diffusion model (Pb(II) metal ions = 50 mg/l, CuO = 0.1 g).

Orders model	Parameters	CuO nanostructures				
		Sample A	Sample B	Sample C	Sample D	Sample E
Pseudo-first-order model	q_e Cal. (mg/g)	1.30	0.23	0.16	1.27	0.31
	q_e Exp. (mg/g)	24.99	24.99	24.985	24.98	24.995
	K_1 (min^{-1})	0.6449	0.476	0.6308	0.0389	0.3573
	R^2	0.967	0.909	0.883	0.982	0.910
Pseudo-second-order model	q_e Cal. (mg/g)	25	25	25.19	24.99	25.16
	q_e Exp. (mg/g)	24.99	24.99	24.98	24.98	24.99
	K_2 (g/mg min)	0.0235	0.0191	0.0525	0.030	0.031
	R^2	0.999	0.999	0.999	0.999	0.999
Intraparticle diffusion model	k_i (mg/g $min^{0.5}$)	0.5205	0.5018	0.0570	0.1264	0.1265
	C (mg/g)	23.64	23.88	24.85	24.66	24.71
	R^2	0.983	0.980	0.896	0.937	0.884

4. Conclusions

CuO nanostructures with different morphologies have been synthesized using microwave heating technique. The produced CuO nanostructures were characterized by XRD, EDX, TEM, and BET. The XRD and EDX patterns confirm that the prepared nanostructures are pure CuO with atomic ratio 1:1 for all samples. In this study, batch adsorption experiments for the removal of Pb(II) from aqueous solutions have been carried out using CuO nanostructures as adsorbent. The adsorption characteristics have been examined at different pH values, contact time and initial metal ion concentrations. The obtained results can be summarized as follows:

- The pH experiments showed that the governing factors affecting the adsorption characteristics of all CuO nanostructures are competition of the H^+ ions with metal ions at low pH values, maximum adsorption at pH 6.5.
- The optimum contact time for adsorption of the heavy metals was considered to be 4 h and after which there was no further adsorption.
- The adsorption experimental results of these heavy metals are in a good correspondence with the Langmuir and Freundlich isotherms.
- All kinetic results suggest that the adsorption of lead (II) by nano structured CuO followed the second-order kinetics model, which relies on the assumption that chemical adsorption may be the rate-limiting step involving valence forces through sharing or exchange of electrons between adsorbent and adsorbate.
- The maximum capacity of oval, cluster, leaves, small rod and porus nanosheets CuO nanostructures for Pb^{2+} are 125, 116, 117, 120 and 115 mg/g. By comparison of the results obtained from this study to the previously reported work on adsorption capacities of various adsorbents in aqueous solution for heavy metal ions, it can be stated that the results of the present work are well.

REFERENCES

Afkhami A, Conway BE. Investigation of removal of Cr (VI), Mo (VI), W (VI), V (IV), and V (V) oxy-ions from industrial wastewaters by adsorption and electrosorption at high-area carbon cloth. J Colloid Interface Sci 2002;251:248–55.

Afkhami A, Madrakian T, Amini A, Karimi Z. Effect of the impregnation of carbon cloth with ethylenediaminetetraacetic acid on its adsorption capacity for the adsorption of several metal ions. J Hazard Mater 2008;150:408–12.

Afkhami A, Madrakian T, Amini A, Karimi Z. Effect of treatment of carbon cloth with sodium hydroxide solution on its adsorption capacity for the adsorption of some cations. Colloids Surf A Physicochem Eng Aspects 2007;304:36–40.

Afkhami A, Moosavi R. Adsorptive removal of Congo red, a carcinogenic textile dye, from aqueous solutions by maghemite nanoparticles. J Hazard Mater 2010;174:398–403.

Aklil A, Mouflih M, Sebti S. Removal of heavy metal ions from water by using calcined phosphate as a new adsorbent. J Hazard Mater 2004;112:183–90.

Alvarez-Ayuso E, Garcia-Sanchez A, Querol X. Purification of metal electroplating waste waters using zeolites. Water Res 2003;37:4855–62.

Cullity B. In: Reading MA, editor. Elements of X-ray diffraction. Addison Wesley Publishing Company; 1978. p. 411–5. 508–522.

Dabrowski A. Adsorption–from theory to practice. Adv Colloid Inter Sci 2001;93(1–3):135.

Demirbas E, Dizge N, Sulak MT, Kobya M. Adsorption kinetics and equilibrium of copper from aqueous solutions using hazelnut shell activated carbon. Chem Eng J 2009;148:480–7.

Dias JM, Alvim-Ferraz M, Almeida FM, Rivera-Utrilla J, Sánchez-Polo. Waste materials for activated carbon preparation and its use in aqueous-phase treatment: a review. J Environ Manag 2007;85:833–46.

Engates KE, Shipley HJ. Adsorption of Pb, Cd, Cu, Zn, and Ni to titanium dioxide nanoparticles: effect of particle size, solid concentration, and exhaustion. Environ Sci Pollution Res 2010;18:386–95.

Feldmann C, Roming M, Trampert K. Polyol-mediated synthesis of nanoscale CaF_2 and CaF_2:Ce, Tb. Small 2006;2(11):1248–50.

Haghseresht F, Lu G. Adsorption characteristics of phenolic compounds onto coal-reject-derived adsorbents. Energ Fuels 1998;12:1100–7.

Hall K, Eagleton L, Andreas Acrivos, Theodore Vermeulen. Pore- and solid-diffusion kinetics in fixed-bed adsorption under constant-pattern conditions. Indus Eng Chem Fund 1966;5:212–23.

Heidari A, Younesi H, Mehraban Z. Removal of Ni (II), Cd (II), and Pb (II) from a ternary aqueous solution by amino functionalized mesoporous and nano mesoporous silica. Chem Eng J 2009;153:70–9.

Hota G, Kumar BR, Ramakrishna S. Fabrication and characterization of a boehmite nanoparticle impregnated

electrospun fiber membrane for removal of metal ions. J Mater Sci 2008;43:212–7.
Jiang M, Wang Q, Jin X, Chen Z. Removal of Pb (II) from aqueous solution using modified and unmodified kaolinite clay. J Hazard Mater 2009;170:332–9.
Langmuir I. The adsorption of gases on plane surfaces of glass, mica and platinum. J Am Chem Soc 1918;40:1361–403.
Liu X, Hu Q, Fang Z, Zhang X, Zhang B. Magnetic chitosan nanocomposites: a useful recyclable tool for heavy metal ion removal. Langmuir 2008;25:3–8.
Low K, Lee C, Leo A. Removal of metals from electroplating wastes using banana pith. Bioresour Technol 1995;51:227–31.
Luisa Cervera M, Carmen Arnal M, de la Guardia M. Removal of heavy metals by using adsorption on alumina or chitosan. Anal Bioanal Chem 2003;375:820–5.
Martinson CA, Reddy K. Adsorption of arsenic (III) and arsenic (V) by cupric oxide nanoparticles. J Colloid Interface Sci 2009;336:406–11.
Mohapatra M, Anand S. Studies on sorption of Cd (II) on Tata chromite mine overburden. J Hazard Mater 2007;148:553–9.
Mohapatra M, Mohapatra L, Singh P, Anand S, Mishra B. A comparative study on Pb (II), Cd (II), Cu (II), Co (II) adsorption from single and binary aqueous solutions on additive assisted nano-structured goethite. Int J Eng Sci Technol 2010;2(8):89–103.
Munagapati VS, Yarramuthi V, Nadavala SK, Alla SR, Abburi K. Biosorption of Cu (II), Cd (II) and Pb (II) by *Acacia leucocephala* bark powder: kinetics, equilibrium and thermodynamics. Chem Eng J 2010;157:357–65.
Naiya TK, Bhattacharya AK, Das SK. Adsorption of Cd (II) and Pb (II) from aqueous solutions on activated alumina. J Colloid Interface Sci 2009;333:14–26.
Ngomsik AF, Bee A, Siaugue JM, Talbot D, Cabuil V, Cote G. Co (II) removal by magnetic alginate beads containing Cyanex 272®. J Hazard Mater 2009;166:1043–9.
Niederberger M, Pinna N. Metal oxide nanoparticles in organic solvents: synthesis, formation, assembly and application. Springer; 2009.
NSC. Lead poisoning available at, http://www.nsc.org/library/facts/lead.htm; 1.9.2007.
Pacheco S, Tapia J, Medina M, Rodriguez R. Cadmium ions adsorption in simulated wastewater using structured alumina-silica nanoparticles. J Non-crystalline Solids 2006;352:5475–81.
Rao MM, Ramana D, Seshaiah K, Wang M, Chang Chien S. Removal of some metal ions by activated carbon prepared from *Phaseolus aureus hulls*. J Hazard Mater 2009;166:1006–13.
Ruparelia J, Duttagupta S, Chatterjee A, Mukherj S. Potential of carbon nanomaterials for removal of heavy metals from water. Desalination 2008;232:145–56.
Santos Yabe MJ, de Oliveira E. Heavy metals removal in industrial effluents by sequential adsorbent treatment. Adv Environ Res 2003;7:263–72.
Sari A, Tuzen M. Biosorption of cadmium (II) from aqueous solution by red algae (*Ceramium virgatum*): equilibrium, kinetic and thermodynamic studies. J Hazard Mater 2008;157:448.
Turker AR. New sorbents for solid-phase extraction for metal enrichment. Clean-Soil Air Water 2007;35:548–57.
Wang J, Chen C. Biosorbents for heavy metals removal and their future. Biotechnol Adv 2009;27:195–226.
Wang JW, Kuo YM. Preparation and adsorption properties of chitosan-poly (acrylic acid) nanoparticles for the removal of nickel ions. J App Polymer Sci 2008;107:2333–42.
Weber W, Morris J. Kinetics of adsorption on carbon from solution. J Sanit Eng Div Am Soc Civ Eng 1963;89:31–60.
Yang M, He J, Hu X, Yan C, Cheng Z. CuO nanostructures as quartz crystal microbalance sensing layers for detection of trace hydrogen cyanide gas. Environ Sci Technol 2011;45:6088–94.
Yin P, Xu Q, Qu R, Zhao G, Sun Y. Adsorption of transition metal ions from aqueous solutions onto a novel silica gel matrix inorganic-organic composite material. J Hazard Mater 2010;173:710–6.
Zhang G, Dong Y, Li X, Wei Y, Shu Q. Effects and mechanisms of oxalate on Cd (II) sorption on goethite at different pH and electrolyte concentration. Plant Nutri Fert Sci 2001;7:305–10.
Zhang W. Nanoscale iron particles for environmental remediation: an overview. J Nanoparticle Res 2003;5:323–32.
Zhu J, Li D, Chen H, Yang X, Lu L, Wang X. Highly dispersed CuO nanoparticles prepared by a novel quick-precipitation method. Mater Lett 2004;58:3324–7.